arXiv:1704.01496v1 [physics.flu-dyn] 5 Apr 2017

Rogue Waves and Large Deviations in Deep Sea

Giovanni Dematteis,[1,2] Tobias Grafke,[1] and Eric Vanden-Eijnden[1]

[1]*Courant Institute, New York University, 251 Mercer Street, New York, NY 10012, USA*
[2]*Dipartimento di Scienze Matematiche, Politecnico di Torino, Corso Duca degli Abruzzi 24, I-10129 Torino, Italy*

(Dated: April 6, 2017)

The appearance of rogue waves in deep sea is investigated using the modified nonlinear Schrödinger (MNLS) equation with random initial conditions that are assumed to be Gaussian distributed, with a spectrum approximating the JONSWAP spectrum obtained from observations of the North Sea. It is shown that by supplementing the incomplete information contained in the JONSWAP spectrum with the MNLS dynamics one can reliably estimate the probability distribution of the sea surface elevation far in the tail at later times. Our results indicate that rogue waves occur when the system hit small pockets of wave configurations hidden in the core of their distribution that trigger large disturbances of the surface height via modulational instability. The rogue wave precursors in these pockets are wave patterns of regular height but with a very specific shape that is identified explicitly, thereby allowing for early detection. The method proposed here builds on tools from large deviation theory that reduce the calculation of the most likely rogue wave precursors to an optimization problem that can be solved efficiently.

Introduction. Rogue waves, long considered a figment of sailor's imagination, are now recognized to be a real, and serious, threat for boats and naval structures such as oil rigs [1, 2]. Oceanographers define them as deep water waves whose crest-to-trough height exceeds twice the significant wave height H_s of the sea, which is itself defined as four times the standard deviation of the surface elevation of the waves in a given sea state. Rogue waves appear rather suddenly and unpredictably, and they can lead to water walls with vertical size on the order of 20–30 m [3, 4], with enormous destructive power. Although rare, they tend to occur more frequently than what one would predict if the sea surface were described by a random Gaussian field [5, 6]. While the mechanisms underlying their appearance remain under debate [7–9], one plausible scenario has emerged over the years: it involves the phenomenon of modulational instability [10, 11], a nonlinear amplification mechanism by which many weakly interacting waves of regular size can create a much larger one. Such an instability arises in the context of the focusing nonlinear Schrödinger (NLS) equation [11–17] or higher order refinements thereof [18–22], which are known to be good models for the evolution of a unidirectional, narrow-banded wave field on the surface of a fluid of infinite depth (that is, a deep sea). Support for the description of rogue waves through such envelope equations recently came from experiments in water tanks [23–26], where Dysthe's modified NLS (MNLS) equation in one spatial dimension [18, 19] was shown to accurately describe the mechanism creating coherent structures which soak up energy from nearby regions. While these experiments and other theoretical works [27, 28] give grounds for the use of MNLS to describe rogue waves, they have not addressed the question of the likelihood of appearance of such waves. Some progress in this direction has been recently made in [29], where a reduced model based on MNLS was used to estimate the probability of a given amplitude within a certain time, and thereby compute the tail of the distribution of the surface height. These calculations were done using an ansatz for the solutions of MNLS, which effectively makes the problem two-dimensional. The purpose of this Letter is to remove this approximation, and study the problem in its full generality. Specifically, we consider the MNLS with random initial data drawn from a Gaussian distribution [30]. The spectrum of this field is chosen to be consistent with the observational record, specifically with the JONSWAP spectrum [31, 32] that describes the empirical distribution of energy among frequencies for a given state of the sea. We calculate the probability of occurrence of a large amplitude solution of MNLS out of these random initial data, and thereby also estimate the tail of the distribution of the sea surface height. These calculations are performed within the framework of large deviation theory (LDT), which predicts the most likely way by which large disturbances arise and therefore also explains the mechanism of rogue wave creation. Our approach is validated by comparison with results from brute-force Monte Carlo simulations, which indicate that rogue waves in MNLS are indeed within the realm of LDT – Monte Carlo simulations are costly, however, and can only be used for waves of moderate amplitude, whereas our approach gives an efficient way to assess the probability of large waves, and importantly allows for a prediction of the tail scaling in the limit of large waves as a function of the sea surface roughness.

Problem setup. Our starting point will be the MNLS equation for the evolution of the complex envelope $u(t,x)$ of the sea surface in deep water [18], in terms of which the surface elevation reads $\eta(t,x) = \Re\big(u(t,x)e^{i(k_0x-\omega_0t)}\big)$ (here k_0 denotes the carrier wave number, $\omega_0 = \sqrt{gk_0}$, and g is the gravitational acceleration). Measuring u and x in units of k_0^{-1} and t in that of ω_0^{-1} we can write MNLS in non-dimensional form as

$$\begin{aligned}&\partial_t u + \tfrac{1}{2}\partial_x u + \tfrac{i}{8}\partial_x^2 u - \tfrac{1}{16}\partial_x^3 u + \tfrac{i}{2}|u|^2 u \\ &+ \tfrac{3}{2}|u|^2\partial_x u + \tfrac{1}{4}u^2\partial_x\bar{u} - \tfrac{i}{2}\,|\partial_x|\,|u|^2 = 0, \quad x\in\Omega,\end{aligned} \tag{1}$$

where $\Omega = [0, L]$ and the bar denotes complex conjugation. We will consider (1) with random initial condition $u_0(x) \equiv u(0,x)$ constructed via their Fourier representation as

$$u_0(x) = \sum_{n\in\mathbb{Z}} e^{ik_nx}(2\hat{C}_n)^{1/2}\zeta_n, \quad \hat{C}_n = Ae^{-k_n^2/(2\Delta^2)}, \tag{2}$$

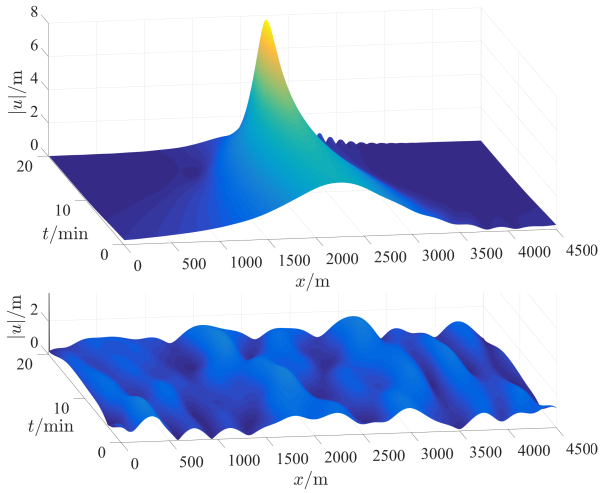

FIG. 1. *Top:* Time evolution of $|u(t,x)|$ starting from an initial condition optimized so that $\max_x |u(T,x)| \geq 8$ m at $T = 20$ min. *Bottom:* Same for a typical Gaussian random initial condition.

where $k_n = 2\pi n/L$, and ζ_n are complex Gaussian variables with mean zero and covariance $\mathbb{E}\zeta_n\bar{\zeta}_m = \delta_{m,n}$, $\mathbb{E}\zeta_n\zeta_m = \mathbb{E}\bar{\zeta}_n\bar{\zeta}_m = 0$. This guarantees that $u_0(x)$ is a Gaussian field with mean zero and $\mathbb{E}(u_0(x)\bar{u}_0(x')) = 2C(x-x') = 2\sum_{n\in\mathbb{Z}} e^{ik_n(x-x')}\hat{C}_n$, where $C(x)$ is the covariance of the surface elevation $\eta_0(x) \equiv \eta(0,x)$. To make contact with the observational data, the amplitude A and the width Δ in (2) are picked so that $\hat{C}_n$ has the same maximum height and area as the JONSWAP spectrum [31, 32].

Because the initial data for (1) are random, so is the solution at time $t > 0$, and our aim is to compute probabilities of the form:

$$P_T(z) \equiv \mathbb{P}\left(F(u(T)) \geq z\right), \tag{3}$$

where $\mathbb{P}$ denotes probability over the initial data, $z \in \mathbb{R}$ is a parameter and F is a scalar functional which depends on the field u at time $T > 0$. Even though our method is applicable to more general F's, here we will focus on

$$F(u(T)) = \max_{x\in\Omega} |u(T,x)| = \max_{x\in\Omega} \eta(T,x)\,, \tag{4}$$

where we used the invariance by a global phase shift to get the second equality.

Large deviation theory. A brute force approach to calculate (3) is Monte Carlo sampling: Generate a large number of realizations of the initial data (2), evolve each of them deterministically via (1) up to time $t = T$, and count the proportion of them that fulfill $F(u(T)) \geq z$. While this method is simple, it is also inefficient when z is large, which is precisely the regime of interest for the tails of the distribution of $F(u(T))$. In that regime, a more efficient approach is to rely on results from LDT which assert that (3) can be estimated by identifying the most likely initial condition that is consistent with $F(u(T)) \geq z$. To see what this entails, recall that the probability density of u_0 is formally proportional to $\exp(-\frac{1}{2}\|u_0\|_C^2)$, where $\|u_0\|_C^2$ is the quadratic form using the inverse of the covariance function $C(x)$ as kernel: in Fourier representation it is explicitly given by

$$\|u_0\|_C^2 = \sum_{n\in\mathbb{Z}} \frac{|\hat{a}_n|^2}{\hat{C}_n}, \quad \hat{a}_n = \frac{1}{L}\int_0^L e^{-ik_n x} u_0(x)dx\,. \tag{5}$$

To calculate (3) we should integrate this density over the set $\mathcal{S} = \{u_0 : F(u(T,u_0)) \geq z\}$, which is hard to do in practice. Instead we can estimate the integral by Laplace's method. This amounts to finding the u_0 that contributes most to the integral via the constrained minimization problem

$$\tfrac{1}{2}\min_{u_0\in\mathcal{S}} \|u_0\|_C^2 \equiv I_T(z)\,, \tag{6}$$

which then yields the following LDT estimate for (3)

$$P_T(z) \asymp z\exp\left(-I_T(z)\right)\,. \tag{7}$$

Here $\asymp$ means that the ratio of the logarithms of both sides tends to 1 as $z \to \infty$, and the factor z in front of the exponential has been added to account for the degeneracy related to invariance of u_0 under a global phase shift.

Numerical aspects. To perform the calculations, we solved (1) with $L = 40\pi$, which is large enough to make the impact of these boundary conditions negligible. We discretized space with 2^{12} gridpoints to resolve the modulational instabilities that arise with (1) and evolved the solution of this equation using a pseudo-spectral second order exponential time-differencing (ETD2RK) method [33, 34]. In the Monte Carlo simulations, we simply picked random ζ_n's in (2) to construct realizations of u_0, evolved them in time, and counted the proportion of them that satisfy $F(u(T)) \geq z$ to estimate $P_T(z)$. In the procedure based on LDT, we performed the constrained minimization over the u_0 using steepest descent with adaptive step (line search) and preconditioning – for details on the numerical scheme, we refer the reader to [35]. In the Monte Carlo simulations and the minimization procedure, we truncated the sums in (2) and (5), respectively, over the $M = 21$ modes with $-10 \leq n \leq 10$: these modes carry most of the variance of u_0 and adding more of them did not affect the results significantly. Note that this implies that the minimization was done in a $2M - 1 = 41$ dimensional space, accounting for invariance by an overall phase shift. Note also that many more modes than the 21 ones present in the initial data emerge in the Fourier transform of $u(t,x)$ via dynamical evolution, which is why we used 2^{12} gridpoints.

Results. We considered two sets of parameters. In Set 1 we took $A = 5.4\cdot 10^{-5}k_0^{-2}$ and $\Delta = 0.19k_0$. Converting back in dimensional variables using $k_0^{-1} = 36$ m, which is a value consistent with the JONSWAP spectrum [31, 32], this means that the significant wave height $H_s = 4\sqrt{C(0)} = 3.3$ m is that of a *rough sea* (using the classification in [36]). It also implies that the Benjamin-Feir index (BFI $= 2\sqrt{2}\sqrt{C(0)}/\Delta$, [32, 37]) is 0.34, meaning that the modulational instability of a typical initial condition is of medium intensity. In Set 2 we took $A = 3.4\cdot 10^{-4}k_0^{-2}$ and $\Delta = 0.19k_0$, for which $H_s = 8.2$ m is that of

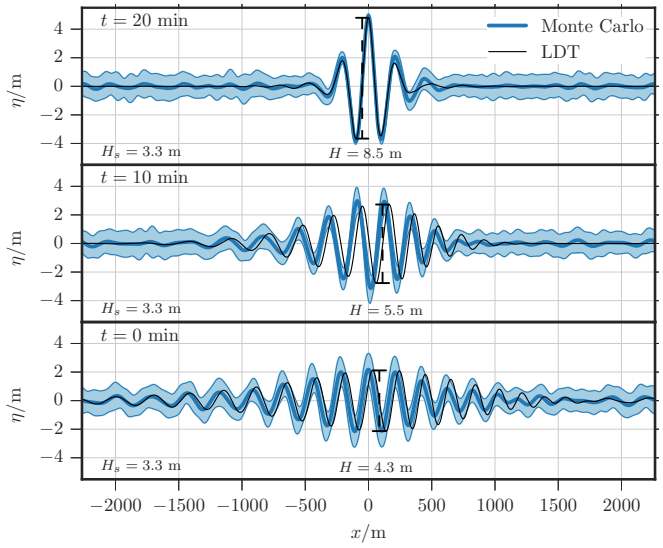

FIG. 2. Comparison between the average of the realizations reaching $\max_x |u(T,x)| \geq 4.8$ m at $T = 20$ min (dark blue) and one standard deviation around this mean (light blue), with the solution reaching the same amplitude starting from the initial condition of maximum likelihood (black). Shown are the surface elevations at initial time $t = 0$, intermediate time $t = 10$ min, and final time $t = 20$ min.

a *high sea* and the BFI is 0.85, meaning that the modulational instability of a typical initial condition is stronger.

Fig. 1 (top) shows the time evolution of $|u(t,x)|$ starting from an initial condition from Set 1 optimized so that $\max_x |u(T,x)| = 8$ m at $T = 20$ min. For comparison, Fig. 1 (bottom) shows $|u(t,x)|$ for a typical initial condition drawn from its Gaussian distribution. To illustrate what is special about the initial conditions identified by our optimization procedure, in Fig. 2 we show snapshots of the surface elevation $\eta(t,x)$ at three different times, $t = 0, 10, 20$ min (black lines), using the constraint that $\max_x |u(T,x)| \geq 4.8$ m at $T = 20$ min. The optimized initial condition has a characteristic oscillation pattern that allows for focusing at the final time. Additionally, we looked at all the Monte Carlo samples that achieve $\max_x |u(t,x)| \geq 4.8$ m, translated them to place their maximum in the center of the domain, and averaged them over. Snapshots of the mean configuration obtained this way are shown in Fig. 2 (blue lines). They agree well with those of the optimized solution (black lines). The one standard deviation spread around the mean of the realizations from Monte Carlo sampling (light blue) is reasonably small, especially around the rogue wave at final time. This indicates that the event $\max_x |u(T,x)| \geq 4.8$ m is indeed realized with probability close to 1 by starting from the most likely initial condition consistent with this event, as predicted by LDT. The usefulness of LDT is confirmed in Figs. 3 (a,b) where we show the probability density functions of the maximal surface elevation for both Sets 1 and 2 calculated via LDT optimization (lines), and compare them to those estimated by Monte Carlo sampling (dots). These densities are related to $P_T(z)$ as $\rho_T(z) = -dP_T/dz$ and they agree accurately in the tail for $\max_x |u(T,x)| \geq H_s$, which roughly marks the onset of the rogue wave regime. Notice however that the Monte Carlo sampling becomes inaccurate in the tail, as expected since the densities are then dominated by unlikely events. The LDT calculation, in contrast, has no difficulty in estimating the densities far in their tail.

The densities plotted in Fig. 3 (a,b) show several remarkable features. First, they indicate that, as T gets larger, the tails of these densities fatten significantly. For example, in Set 1 $\rho_T(z) \approx 5 \cdot 10^{-5}$ for $z = 6$ m at $T = 20$ min, which is 4 order of magnitude larger than what it was initially since $\rho_{T=0}(z) \approx 5 \cdot 10^{-9}$ for $z = 6$ m at $T = 0$ – we will come back below on the implications this has on the probability to observe a rogue wave within a time window. A second interesting property of the densities shown in Fig. 3 (a,b) is that they converge to a limiting density as T gets larger. This occurs after some decorrelation time $\tau_c \approx 10$ min in Set 1 and $\tau_c \approx 3$ min in Set 2. Similarly, the optimization procedure used in the LDT approach also converges: in fact, this convergence can be observed at the level of the trajectories generated from the optimal $u_0^\star$. As Fig. 3 (c) shows, if we read these trajectories backward from $t = T$, we see that their end portions coincide, regardless on whether we took $T = 20$ min, $T = 15$ min, or $T = 10$ min in Set 1 and a similar phenomenon is observed in Set 2.

Discussion. The convergence of $P_T(z)$ towards some limiting function $P(z)$ has important consequences for the significance and interpretation of our method and the results it gives. To see why, notice first that this convergence can be explained if we assume that the probability distribution of the solutions to (1) with Gaussian initial data converge to some invariant measure. In this case, after a while (i.e. for T large enough) the Monte Carlo simulations will sample the value of $\max_x |u|$ on this invariant measure, and the optimization procedure based on LDT will do the same. The timescale over which convergence occurs (i.e. the value of τ_c) depends on how close the initial Gaussian measure we took for $u_0(x)$ is from this invariant measure. Interestingly the estimate for τ_c is in rough agreement with the time scale over which a modulational instability develops from a random Gaussian initial condition with root mean square amplitude $\sqrt{C(0)}$. Indeed, a simple dimensional argument using to estimate the time scale associated with the term $\frac{i}{2}|u|^2 u$ mainly responsible for the modulational instability in (1) gives (using $2C(0)$ as typical amplitude for $|u|^2$ and going back to dimensional variables for convenience) $\tau_{\text{mod}} = 1/(2\omega_0 k_0^2 C(0)) \approx 30$ min in Set 1 and $\tau_{\text{mod}} \approx 5$ min in Set 2.

These findings indicate that, even though the assumption that $u_0(x)$ is Gaussian is incorrect in the tail (that is, $P_{T=0}(z)$ is not equal to the limiting $P(z)$ in the tail), it contains the right seeds to estimate $P(z)$ via $P_T(z)$ if $T \gtrsim \tau_c$ [38]. Altogether this is consistent with the scenario put forward by Sapsis and collaborators in [39] to explain how extreme events arise in intermittent dynamical systems and calculate their probability: they occur when the system hits small instability pockets

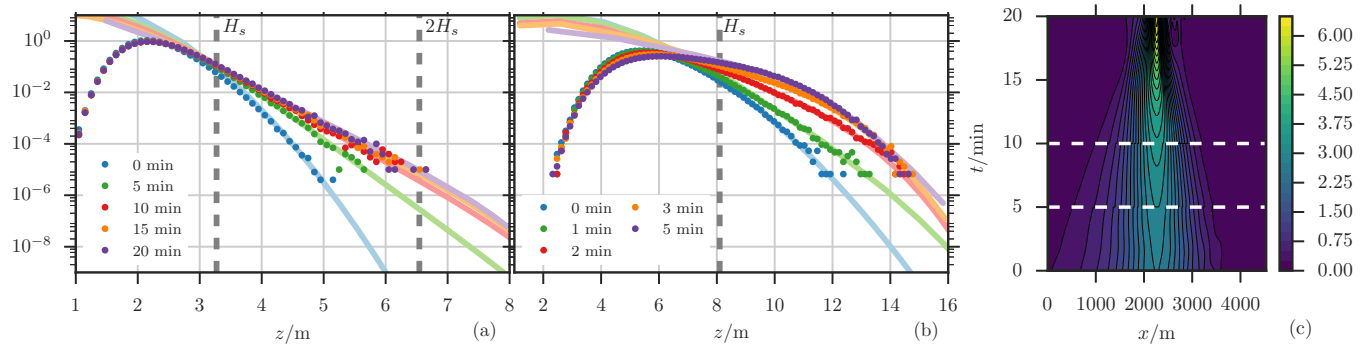

FIG. 3. Probability densities $\rho_T(z)$ of the maximal surface elevation, $\max_x \eta(T,x)$, for different times T for Set 1 (a) and Set 2 (b). The densities estimated by direct sampling via Monte Carlo (dots) are compared with those predicted by LDT (lines). These densities agree over about 5 orders of magnitude in probability, though LDT allows for the calculation of the tail where Monte Carlo becomes very costly. The dashed line at H_s represents the onset of the Rogue wave regime. Also shown in (c) is a contourplot of the optimal trajectories from LDT for $T = 10$, 15, and 20 min in Set 1. The trajectories are superposed so that they match at $t = T$, and read backward from there. These trajectories coincide, which is consistent with the convergence of the probability densities $\rho_T(z)$ for large T.

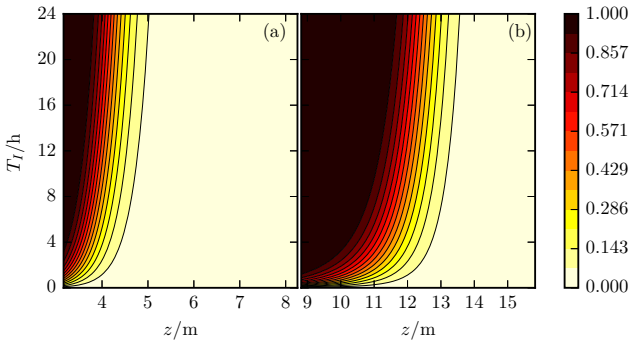

FIG. 4. Contourplots of the probability to observe a wave whose amplitude exceeds z in the time window $[0, T_I]$ for Sets 1 (a) and 2 (b).

in the core of its distribution which trigger a large transient excursion. In this scenario, as long as the initial distribution is accurate in the core, the dynamics will permit precise estimation of its tail. In some sense, the distribution of the initial condition plays a role similar to the prior distribution in Bayesian inference [40], and the posterior can be effectively sampled by adding the additional information from the dynamics over relatively short period of time during which these instabilities can occur. In [39], this picture was made predictive by using a two-dimensional ansatz for the initial condition $u_0(x)$. What our results show is that this approximation can be avoided altogether by using LDT to perform the calculations directly with the full Gaussian initial condition (2).

Interestingly, we can use the results above to calculate the probability of occurrence of rogue waves in a given time window. More precisely, the probability $p(z, T_I)$ that no rogue wave of amplitude larger than z be observed in the domain Ω during $[0, T_I]$ (i.e. that $\max_{t\in[0,T_I]} \max_{x\in\Omega} |u(t,x)| \leq z$) can be estimated in terms of $P(z)$ and τ_c as

$$p \equiv \mathbb{P}\Big(\max_{t\in[0,T_I]} \max_{x\in\Omega} |u(t,x)| \leq z \Big) \sim [1 - P(z)]^{T_I/\tau_c}, \quad (8)$$

where we used the fact that rogue waves can be considered independent on timescales larger than τ_c and we assumed that $T_I \gg \tau_c$. The function $1 - p$ is plotted in Fig. 4 as a function of z and T_I. For example, using the parameters of Set 1, (8) indicates that there is a 50% chance to observe a rogue wave of height $z = 4$ m (that is, about 8 m from crest-to-trough) after 11 hours (using $\tau_c = 10$ min and $P(z = 4\text{ m}) = 1.1 \cdot 10^{-2}$); if we wait 30 hours, the chance goes up to 85%. Similarly, for Set 2 the chance to observe a wave of 11 m height is about 50% after 3 hours and about 85% after 8 hours ($\tau_c = 3$ min and $P(z = 11\text{ m}) = 1.2 \cdot 10^{-2}$).

Concluding remarks. We have shown how an optimization problem building on LDT can be used to predict the pathway and likelihood of appearance of rogue waves in the solutions of MNLS fed by random initial data consistent with the available observational data. This setup guarantees that the core of the distribution with which we initiate MNLS is accurate, which in turn permits the precise estimation of its tail via the dynamics. Our results are consistent with the picture in which modulational instabilities are the culprit for the creation of rogue waves, and they give quantitative estimate for the probabilities of observing waves of a given amplitude within a given time window. These results also show that rogue waves have very specific precursors, a feature that could potentially be used for their early detection.

Acknowledgments. We thank W. Craig for helpful discussions, and M. Onorato, M. Mohamad, and T. Sapsis for interesting comments. GD is supported by the joint Math PhD program of Politecnico and Università di Torino. EVE is supported in part by the Materials Research Science and Engineering Center (MRSEC) program of the National Science Foundation (NSF) under award number DMR-1420073 and by NSF

under award number DMS-1522767.

[1] P. Müller, C. Garrett, and A. Osborne, Oceanography **18**, 66 (2005).
[2] B. S. White and B. Fornberg, J. Fluid Mech. **355**, 113 (1998).
[3] S. Haver, Rogue waves 2004 , 1 (2004).
[4] I. Nikolkina and I. Didenkulova, Nat. Hazards Earth Syst. Sci. **11**, 2913 (2011).
[5] M. Onorato, S. Residori, U. Bortolozzo, A. Montina, and F. Arecchi, Phys. Rep. **528**, 47 (2013).
[6] S. Nazarenko and S. Lukaschuk, Annu. Rev. Condens. Matter Phys. **7**, 61 (2016).
[7] N. Akhmediev, J. M. Soto-Crespo, and A. Ankiewicz, Physics Letters A **373**, 2137 (2009).
[8] N. Akhmediev and E. Pelinovsky, Eur. Phys. J. Special Topics **185**, 1 (2010).
[9] M. Onorato, D. Proment, G. El, S. Randoux, and P. Suret, Phys. Lett. A **380**, 3173 (2016).
[10] T. B. Benjamin and J. E. Feir, J. Fluid Mech. **27**, 417 (1967).
[11] V. E. Zakharov, J. Appl. Mech. Tech. Phys. **9**, 190 (1968).
[12] N. Akhmediev, V. Eleonskii, and N. Kulagin, Theoretical and mathematical physics **72**, 809 (1987).
[13] E. A. Kuznetsov, Akademiia Nauk SSSR Doklady **236**, 575 (1977).
[14] D. H. Peregrine, The ANZIAM Journal **25**, 16 (1983).
[15] A. R. Osborne, M. Onorato, and M. Serio, Phys. Lett. A **275**, 386 (2000).
[16] V. E. Zakharov and L. A. Ostrovsky, Physica D **238**, 540 (2009).
[17] M. Onorato, T. Waseda, A. Toffoli, L. Cavaleri, O. Gramstad, P. Janssen, T. Kinoshita, J. Monbaliu, N. Mori, A. R. Osborne, *et al.*, Phys. Rev. Lett. **102**, 114502 (2009).
[18] K. B. Dysthe, Proc. R. Soc. Lond. A **369**, 105 (1979).
[19] M. Stiassnie, Wave motion **6**, 431 (1984).
[20] K. Trulsen and K. B. Dysthe, Wave motion **24**, 281 (1996).
[21] W. Craig, P. Guyenne, and C. Sulem, Wave Motion **47**, 552 (2010).
[22] O. Gramstad and K. Trulsen, J. Fluid Mech. **670**, 404 (2011).
[23] M. Onorato, A. Osborne, M. Serio, L. Cavaleri, C. Brandini, and C. Stansberg, Phys. Rev. E **70**, 067302 (2004).
[24] A. Chabchoub, N. Hoffmann, and N. Akhmediev, Phys. Rev. Lett. **106**, 204502 (2011).
[25] A. Chabchoub, N. Hoffmann, M. Onorato, and N. Akhmediev, Phys. Rev. X **2**, 011015 (2012).
[26] A. Goullet and W. Choi, Phys. Fluids **23**, 016601 (2011).
[27] E. Lo and C. C. Mei, J. Fluid Mech. **150**, 395 (1985).
[28] W. Cousins and T. P. Sapsis, Phys. Rev. E **91**, 063204 (2015).
[29] W. Cousins and T. P. Sapsis, J. Fluid Mech. **790**, 368 (2016).
[30] S. Nazarenko, *Wave turbulence*, Vol. 825 (Springer Science & Business Media, 2011).
[31] K. Hasselmann, T. P. Barnett, E. Bouws, H. Carlson, D. E. Cartwright, K. Enke, J. A. Ewing, H. Gienapp, D. E. Hasselmann, P. Kruseman, *et al.*, *Measurements of wind-wave growth and swell decay during the Joint North Sea Wave Project (JONSWAP)*, Tech. Rep. (Deutches Hydrographisches Institut, 1973).
[32] M. Onorato, A. R. Osborne, M. Serio, and S. Bertone, Phys. Rev. Lett. **86**, 5831 (2001).
[33] S. M. Cox and P. C. Matthews, J. Comp. Phys. **176**, 430 (2002).
[34] A.-K. Kassam and L. N. Trefethen, SIAM J. Sci. Comput. **26**, 1214 (2005).
[35] G. Dematteis, T. Grafke, and E. Vanden-Eijnden, "Rogue waves and large deviations in (M)NLS with random initial data," (2017), in preparation.
[36] W. M. Organization, ed., *Manual on Codes - International Codes, Volume I.1, Annex II to the WMO Technical Regulations: part A- Alphanumeric Codes*, WMO- No. 306 (Secretariat of the World Meteorological Organization, 2016).
[37] P. A. E. M. Janssen, J. Phys. Oceanogr. **33**, 863 (2003).
[38] Note that this convergence occurs on the timescale τ_c which is much smaller than the mixing time for the solutions of (1), i.e. the time it would take from a given initial condition, rather than an ensemble thereof, to sample the invariant measure. To make this invariant measure consistent with the JONSWAP spectrum would possibly require adding appropriate forcing and dissipation terms in (1)) that act on time scales much longer than τ_c. We avoid this problem by taking a initial distribution that already contains the right information.
[39] M. A. Mohamad, W. Cousins, and T. P. Sapsis, J. Comp. Phys. **322**, 288 (2016).
[40] Note in particular that the Gaussian (2) is the random field that maximizes entropy given the constraint on its covariance $C(x)$.